

Impact of Different End Region Cooling Arrangements on Endwinding Heat Transfer Coefficients in Electric Motors

A. Boglietti⁽¹⁾, *Senior Member, IEEE*, A. Cavagnino⁽¹⁾, *Member, IEEE*,

D.A. Staton⁽²⁾, *Member, IEEE*, M. Popescu⁽²⁾, *Senior Member, IEEE*

⁽¹⁾ Politecnico di Torino, Dipartimento di Ingegneria Elettrica, 10129 Torino, ITALY

⁽²⁾ Motor Design Ltd, Ellesmere, Shropshire, SY12 OEG, UK

Abstract – In this paper the impact of different end region cooling arrangements on the endwinding heat transfer is analyzed. An experimental approach to the problem solving has been adopted: two “ad hoc” prototypes have been built, and a test bench has been assembled. Open Drip Proof “ODP” and Total Enclosed Fan Cooled “TEFC” frames have been taken into account. In addition the cooling effect of the fins always present in the induction motor cage end-rings have been analyzed too. The paper reports in detail the set up of the test procedures and the obtained results. Particular care has been devoted to the determination of the heat transfer coefficients concerning the thermal transfer between endwinding and external frame. The obtained results are of basic importance for the determination of the thermal resistances between endwindings and end caps to be utilized in thermal networks usually adopted in thermal model analysis.

Keywords: induction motors, thermal model, parameter identification, endwinding cooling, and heat transfer coefficients.

I. INTRODUCTION

The use of devoted software for the thermal analysis of induction motors has become popular [1]. Thermal analysis and electromagnetic design tools, when used in conjunction, provide important verification prior to moving to prototype realizations. This approach allows a cost saving in progression from the initial design to device production. In addition, the thermal analysis becomes essential in reducing the laboratory time-consuming cost for thermal verification tests. The accuracy of a thermal analysis, based on lumped parameter thermal network, is dependant on the accuracy of the thermal resistance computation and, as a consequence, on the accuracy of the available heat transfer coefficients linked to the natural and the forced convection heat exchange inside and outside the motor [1]. With reference to induction motors, in this paper the effect of different arrangements on the endwinding cooling and the related heat transfer coefficients have been obtained by means of a full experimental approach [2], [7]. Although the presented activities concern induction motors, the obtained results have general validity and they can be used for thermal analysis of different radial flux motors, such as permanent magnet, synchronous reluctance machine, etc.

II. THERMAL PHENOMENA AND RELATED PROBLEMS

Due to the large number of thermal exchanges simultaneously active, the thermal phenomena inside an electrical motor are very complex. In fact, conduction, natural convection, forced convection and radiation are all present with a relative weight that depends on the motor cooling system (natural convection, fan cooling, water cooling, and so on). In addition, many heat sources are active at the same time. As a consequence, it is not easy to split the causes and effects in thermal exchange phenomena. The most widely used procedure to analyze these heat transfer exchanges is the definition of thermal networks based on lumped parameters, as shown in a rich technical literature on this topic (see reference list in [1]). The most difficult aspect of this approach is the correct determination of heat transfer coefficients and the resulting thermal resistances for convection and radiation heat transfer. When using an experimental approach to help quantify heat transfer coefficients, the use of a standard motor is often not the best choice, in particular when a single thermal effect has to be analyzed [3]-[6]. As a consequence, in the proposed approach, suitable induction motor prototypes have been designed and built [2], [7].

III. TEST BENCH AND MOTOR PROTOTYPES

In a complex system the thermal phenomena analysis can be simplified where, as far as possible, the heat sources can be separately activated. In particular, when the stator winding cooling effects are under analysis, it is convenient that only the stator joule losses should be present and the other thermal sources should not be active. Obviously, this condition is particularly true when the phenomena involved in the endwinding cooling are to be studied [2]. For this reason, two “ad hoc” prototypes have been built and utilized.

The first prototype is a standard 2 poles Total Enclosed Fan Cooled “TEFC” motor (Motor A in this paper), while the second one is a 4 poles Open Drip Proof “ODP” (Motor B in this paper). For increasing the cooling effects of the endwindings, some openings are present in the main frame and in the two end-caps of this motor. Since only the inner cooling effect on the endwinding must be active, the external fan of Motor A has been removed.

TABLE I
NAME PLATE DATA OF THE PROTOTYPES

| Motor prototype | Motor A | Motor B |
|----------------------------------|---------|----------|
| Original motor rated power, [HP] | 3 | 5 |
| Enclosure type | TEFC | ODP |
| Frequency, [Hz] | 60 | 60 |
| Rated Voltage, [V] | 230/460 | 230/460 |
| Rated current, [A] | 8.0/4.0 | 13.4/6.7 |
| Pole number | 2 | 4 |
| Rated speed, [rpm] | 3530 | 1760 |
| Rated efficiency, [%] | 88.5 | 87.5 |
| Endwinding over-length, [mm] * | 48 | 45 |
| Endwinding perimeter, [mm] ** | 108 | 90 |
| Endwinding average diameter [mm] | 145 | 150 |

* Over length from the lamination of a single endwinding in axial direction

** Perimeter of the endwinding cross section

In the two motors, the rotor laminations and the rotor squirrel cages have been totally replaced by a nylon cylinder, as shown in Fig.1. In order to maintain the internal ventilation effect, the two end rings of the original rotors have been fixed by screws on the two sides of the plastic cylinder, as seen in Fig.2. The plastic rotor diameter has been turned to maintain the same value as the original one. The adopted motor code and the rated data of the two prototypes are reported in Table I. Fig.3 shows the TEFC Motor A on the left side and the ODP Motor B in the right side. In the bigger rotor (Motor B), very long end ring fins are adopted (as evident in Fig.1) to improve the endwindings ventilation. Conversely, the small rotor (Motor A) has regular end ring fins, as usually adopted in this machine type.

The two motors are not monitored by thermal sensors, but the winding temperatures can be self monitored during the tests as described in section IV, while the stator lamination temperature can be measured by a digital thermometer through a hole available inside the terminal box for both the motors. Due to the plastic rotors, the two motors cannot rotate by themselves, so the two rotors are mechanically connected to an industrial TEFC induction motor (in the following called "Drive Motor") using the mechanical output shafts of this machine. In particular, the regular output shaft is connected to one motor under test while the shaft on the other side is connected to the second prototype removing the external fan and cowling of the Drive Motor. In Fig.4, the complete test bench is shown. The two motors under test have both been connected to the Drive Motor because this configuration allows performing the thermal tests on the two machines at the same time, halving the number of tests. In order to introduce a high thermal resistance between the three shafts, the two mechanical joints have been realized using a simple rubber water-pipe. This joint does not present problems because a very small torque due to the mechanical losses is involved only. In addition, the rubber water-pipe joints introduce a thermal disconnection, reducing the thermal flux from one motor to the other. As a consequence, the three motors can be considered thermally decoupled. This configuration minimizes the ventilation effects on the prototype endcaps that could be introduced by traditional mechanical joints.

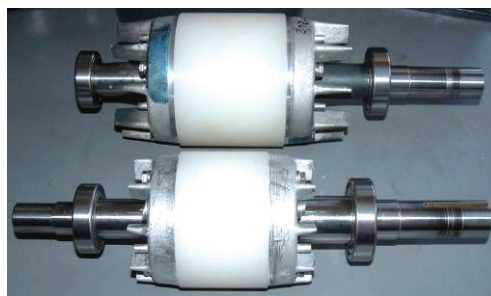


Fig.1: Prototype plastic rotors
(Motor A bottom and Motor B top).

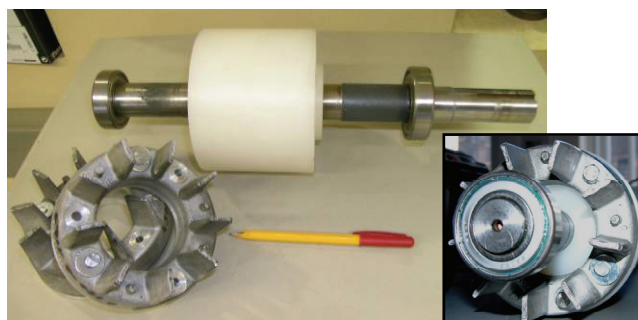


Fig.2: End ring positioning on the plastic rotor.



Fig. 3: TEFC Motor A (left) and ODP Motor B (right).



Fig. 4: Test bench with the two motors under test
(Motor B in TEFC configuration).

In order to increase the thermal decoupling, a plastic barrier is introduced between the Drive Motor and Motor A, as shown in Fig.4. The aim of the plastic barrier is to stop the air flow produced by Motor B versus Motor A. An inverter is used to supply the Drive Motor, in order to impose the requested

speed to the two plastic rotors. The test bench has been positioned in a room with ambient temperature variation lower than 2 °C throughout the day. The test rig has been positioned on a wood support to reduce the thermal exchange through the motor feet.

IV. EXPERIMENTAL TEST DESCRIPTION

Using the previously described test bench the following tests have been performed on each prototype:

- Thermal test with a DC supply connecting the three windings in series and with the rotor still. This test is the reference condition for the thermal models set up.
- Thermal test with a DC supply connecting the three windings in series and with the rotor running at constant speed imposed by the Drive Motor. In particular the following mechanical speeds have been considered: 250, 500, 750, 1000, 1500, 2000, and 2500 rpm.

In order to provide evidence of the cooling effects due to the end ring fins, Motor A has been tested with and without end rings. Removing the end rings from the plastic cylinder should reduce the inner ventilation effect. Motor B has been tested considering the original “ODP” enclosure and a TEFC enclosure obtained by closing all the frame and end caps openings with plastic tape, as shown in Fig. 4. In addition, a third test condition without rotor end rings has been represented by considering the plastic cylinder only, as shown in Fig. 2.

The use of a DC supply involves stator joule losses only, simplifying the thermal analysis. In fact, with a sinusoidal supply, the loss contribution values are not known accurately and the loss separation is made following international standards. In DC supply conditions the thermal system is more obvious and an easier thermal analysis can be adopted. In addition, knowing the winding resistance at a reference temperature, with a DC supply the ratio between the voltage and current allows continuous monitoring of the winding temperature during the temperature test. In order to avoid motor damage, the DC supply voltage for the two motors has been chosen to inject an appropriate constant DC power of 100 W for Motor A and 150 W for Motor B. These powers lead to an overtemperature rise (about 70-80 °C for both the prototypes) compatible with the motor insulation class. It is important to remember that during the tests the prototypes are without any type of external ventilation.

In the tests, the stator winding, stator lamination and external motor frame temperatures have been measured in thermal steady state condition, together with the ambient temperature. The external motor frame temperature is the average values of 25 measured temperatures on the main frame and on the end caps, as described in [7].

V. THERMAL MODEL REMARKS

Very simplified thermal models can be used to analyze the thermal behaviors of the prototypes. These models have been proposed and verified in [7] both for the ODP and TEFC enclosure type.

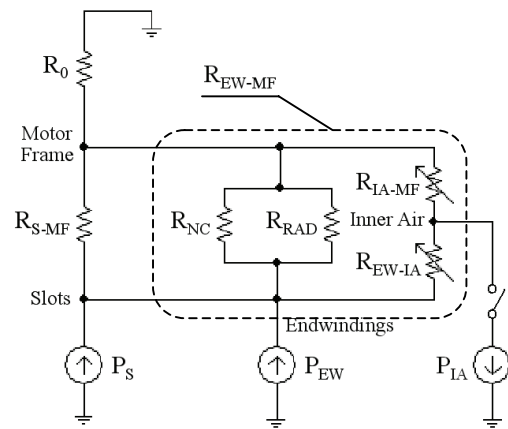


Fig. 5: Simplified thermal models: Model 1 for TEFC machine (open switch) and Model 2 for ODP machine (closed switch).

TABLE II
MEANING OF THE SYMBOLS USED IN FIG.5

| Symbol | Meaning |
|-------------|--|
| P_S | Stator winding joule losses (active conductors in the slots) |
| P_{EW} | Stator winding joule losses (end windings) |
| P_{IA} | Losses removed from the end regions by the air flow in the enclosure openings (active in the Model 2 only). |
| R_0 | Thermal resistance between motor frame and ambient |
| R_{S-MF} | Conduction thermal resistance between the copper in the slot and the motor frame (estimated as reported in [7]) |
| R_{NC} | Thermal resistance between endwindings and motor frame due to natural convection |
| R_{RAD} | Thermal resistance between endwindings and motor frame due to radiation |
| R_{EW-IA} | Thermal resistance between endwindings and the inner air |
| R_{IA-MF} | Thermal resistance between inner air and the motor frame |
| R_{EW-MF} | In the Model 1 it is the thermal resistance between endwindings and the motor frame (parallel of R_{NC} , R_{RAD} and R_{EW-IA} plus R_{IA-MF}) |

For convenience the models proposed in [7] are reported in Fig.5. Fig.5 describes the model for TEFC machine (labelled as Model 1) when the switch is open, while it can be used to analyze ODP enclosures when the switch is closed (Model 2). The meaning of the symbols used in Fig.5 are listed in Table II. Model 1 has been used to study the Motor A and the Motor B when its frame openings are closed (TEFC configuration). For the Motor B in original configuration, both the Models can be used to analyze the machine [7].

Since the complete step-by-step procedure to evaluate the thermal resistances and the heat transfer coefficients related to the end space regions of the considered prototypes is reported in [7], hereafter only the obtained results will be reported. However, it is opportune to describe this procedure in outline. Starting from the stator winding and the external motor frame steady state temperatures and knowing the injected power, all the thermal resistances of the thermal network of Fig.5 can be calculated. Since the endwindings and inner end caps surfaces are known, the required heat transfer coefficients can be easily evaluated.

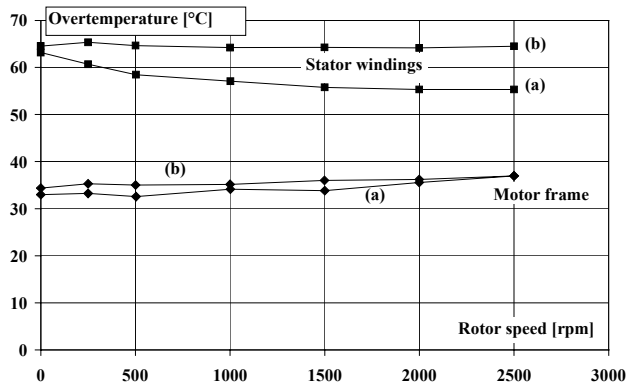


Fig. 6: Stator winding and motor frame overtemperature versus the rotor speed for the Motor A: (a) with end rings, (b) without end rings.

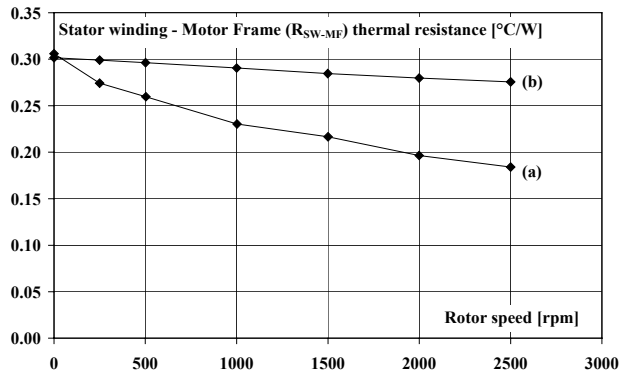


Fig. 7: Thermal resistance between the stator winding and the motor frame vs. rotor speed for the Motor A: (a) with end rings, (b) without end rings.

VI. EXPERIMENTAL AND COMPUTED RESULTS

A. Motor A Results

Fig. 6 shows the stator winding and motor frame steady state overtemperature versus the rotor speed for the Motor A. In this figure the letter (a) refers to tests with end rings and the letter (b) is used for tests where the end rings were removed by the plastic cylinder. It is possible to observe that without the end rings the winding cooling is less efficient, while there are not appreciable effects on the motor frame overtemperature. The small rise in temperature of the motor frame at high speed is due to the increase of the bearing mechanical losses and the increase of the ventilation losses inside the closed end caps.

The thermal resistance between the stator winding and the motor frame R_{SW-MF} (equal to the parallel of the R_{S-MF} and R_{EW-MF} resistances shown in Fig.5, Model 1) is reported in Fig. 7. Also in this case the effect of the inner ventilation due to the end ring fins is evident. As a consequence, very different values for the forced convection thermal resistances between the endwindings and the motor frame are expected with respect to the tested rotor configurations. The results reported in Fig. 8 confirm this expectation.

The heat transfer coefficients between the endwinding and the motor frame have been evaluated as reported in [7]. The obtained results are shown in Fig.9 and Fig.10.

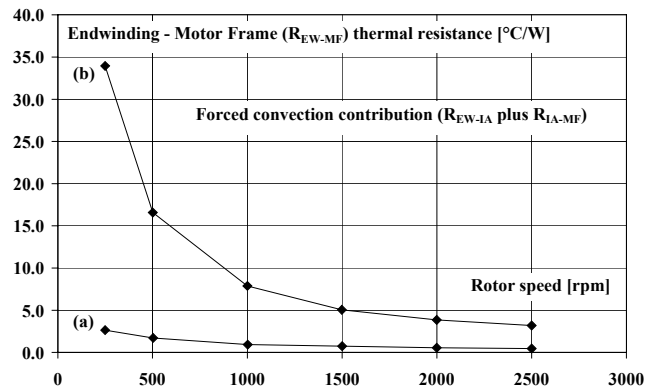


Fig. 8: Thermal resistance between the endwinding and the motor frame versus rotor speed for the Motor A: (a) with end rings, (b) without end rings.

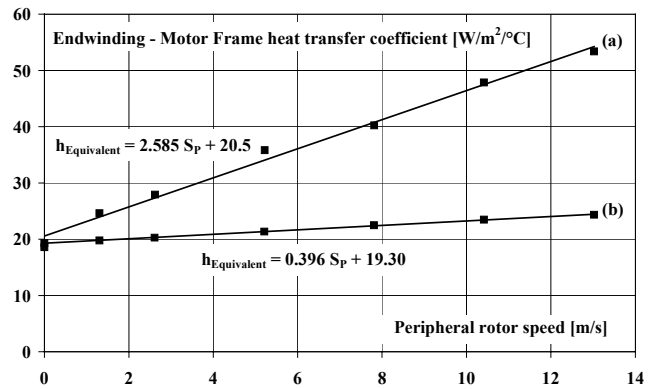


Fig. 9: Endwinding – motor frame equivalent heat transfer coefficient for the Motor A: (a) with end rings, (b) without end rings.

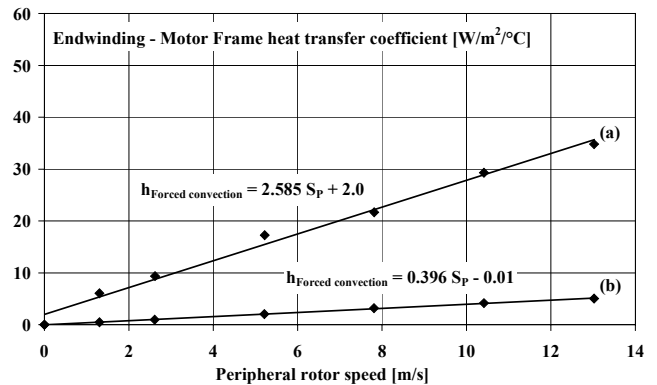


Fig. 10: Endwinding – motor frame forced convection heat transfer coefficient for the Motor A: (a) with end rings, (b) without end rings.

In these two figures the equivalent (taking into account natural convection, radiation and forced convection phenomena in the inner air end regions) and forced convection heat transfer coefficients as function of the peripheral rotor speed are reported respectively. In particular, Fig.10 highlights that the forced convection heat transfer coefficient values become negligible when the rotor rings are not present. This fact confirms the importance of the fins realized on the rotor end rings for an effective endwinding cooling.

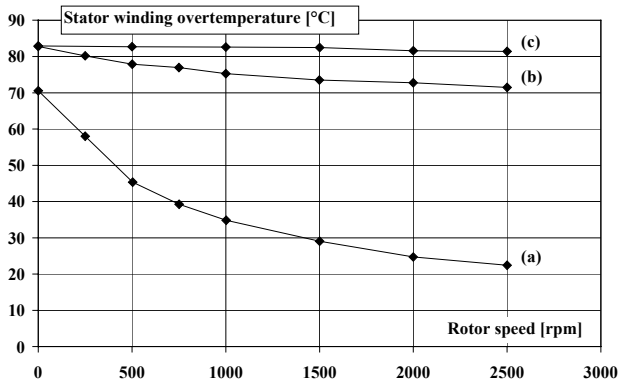


Fig. 11: Stator winding overtemperature for the Motor B: (a) original configuration, (b) with closed frame openings, (c) as (b) without end rings.

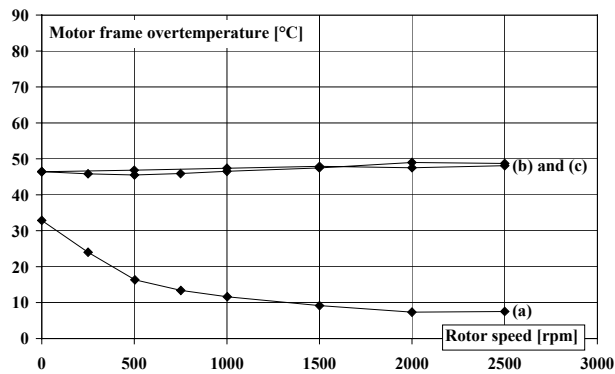


Fig. 12: Stator winding overtemperature for the Motor B: (a) original configuration, (b) with closed frame openings, (c) as (b) without end rings.

B. Motor B Results - Model 1

The motor B has been tested in three conditions. In the figures concerning this machine three letters are used to identify the test type. In particular: (a) for the Motor B with open frame openings and with end rings (original configuration, Fig.3), (b) for the prototype with closed frame openings (Fig.4) and with end rings positioned on the plastic rotor (Fig.1) and (c) when the frame openings have been closed (Fig.4) and the end rings removed by the plastic cylinder (Fig.2).

The different endwinding cooling arrangements have been initially analyzed using the Model 1. This is correct when the motor enclosure is of TEFC type, but it can be questionable when the frame openings are open. In fact, for ODP enclosure model 2 has to be used. However, as explained in [7], Model 1 applied to ODP enclosures models the heat removal through the frame openings as a fictitious reduction of the natural convection thermal resistance R_0 between the external frame and the ambient (see Fig.17) and the obtained results seem to be reasonable. The effects of the passage from ODP to TEFC enclosure type are shown in Fig.11 and Fig.12, where the stator winding and motor frame temperatures are reported as a function of the rotational speed. It is interesting to observe that with the rotor still and closed frame openings both the stator winding and the motor frame overtemperatures increase about 12 °C with respect to the original frame configuration.

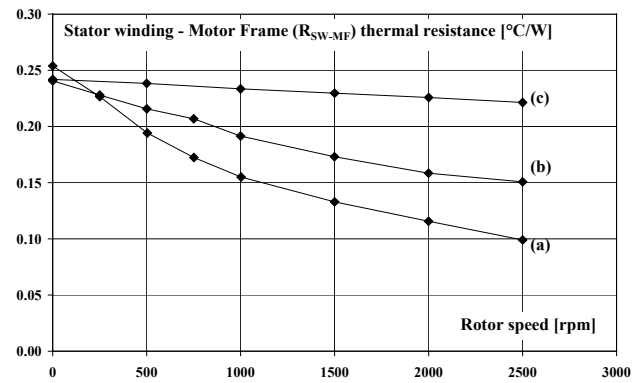


Fig. 13: Motor B stator winding-motor frame thermal resistance: (a) original configuration, (b) with closed frame openings, (c) as (b) without end rings.

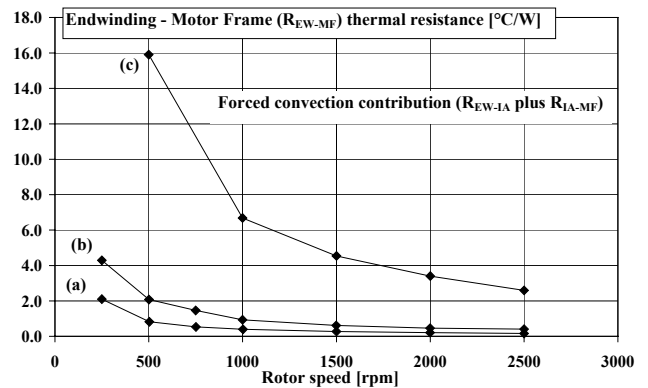


Fig. 14: Motor B endwinding-motor frame forced convection thermal resistance: (a) original configuration, (b) with closed frame openings, (c) as (b) without end rings.

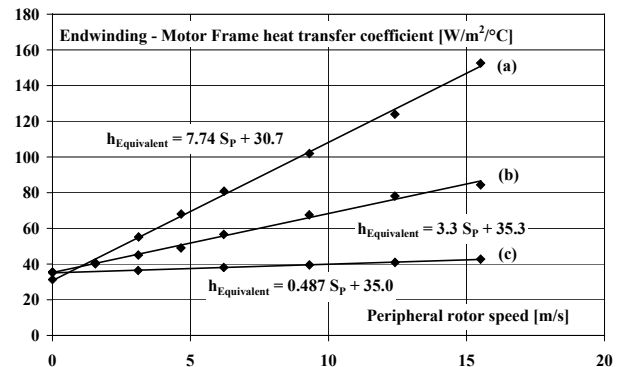


Fig. 15: Endwinding - motor frame equivalent heat transfer coefficient for the Motor B: (a) original configuration, (b) with closed frame openings, (c) as (b) without end rings.

When the machine is configured as a TEFC one, Fig.11 and Fig.12 lead to the same considerations previously reported for the Motor A. In Fig.13 and Fig.14 the thermal resistances influenced by the inner air cooling are reported. Starting from these values, the heat transfer coefficients related to the heat exchange in the end space regions have been calculated. In particular, the equivalent heat transfer coefficient as a function of the peripheral rotor speed is shown in Fig. 15 and the forced convection one is reported in Fig.16.

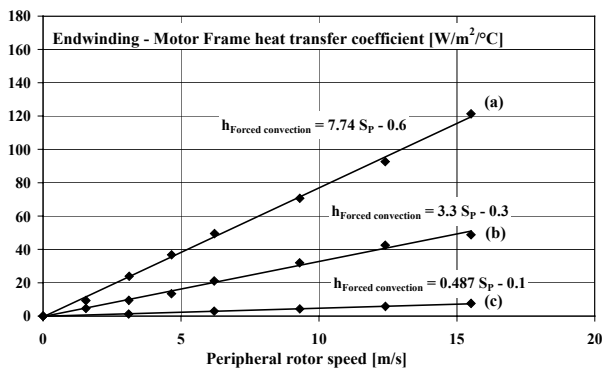


Fig. 16: Endwinding – motor frame forced convection heat transfer coefficient for the Motor B: (a) original configuration, (b) with closed frame openings, (c) as (b) without end rings.

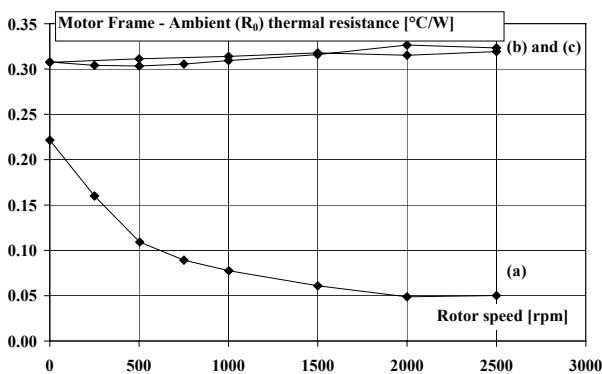


Fig. 17: Thermal resistance between motor frame and ambient for the Motor B: (a) original configuration, (b) with closed frame openings, (c) as (b) without end rings.

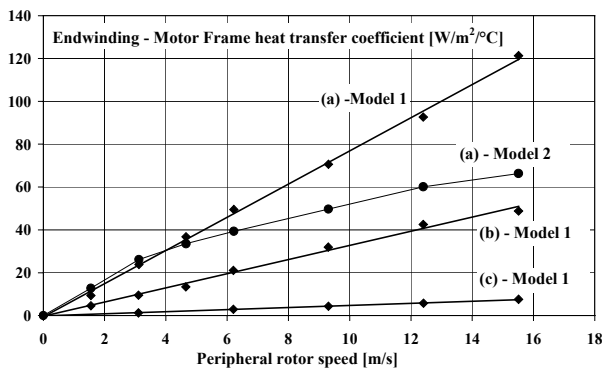


Fig. 18: Endwinding forced convection heat transfer coefficient comparison using Model 1 and Model 2 for the Motor B: (a) original configuration, (b) with closed frame openings, (c) as (b) without end rings

Comparing Fig.16 and Fig.10, it is possible to observe that the obtained values for the (c) configuration (Motor B in TEFC configuration without the end rings) are practically equal to the values estimated for the Motor A without the end rings (line (b) in Fig.10). This confirms both the measurement accuracy and the goodness of the proposed experimental approach for endwinding heat transfer coefficient estimation.

B. Motor B Results - Model 2

The thermal resistance R_0 between the frame and the ambient (taking into account natural convection and radiation) is shown in Fig.17. This resistance is defined as the ratio between the motor frame overtemperature and the total

injected power in the winding. It is evident that R_0 is relatively/almost constant when the frame openings are closed, while it decreases when the rotor speed when the openings are open. This fact is physically questionable because it is necessary to take into account the heat removal by the air flux in the openings. For this reason the authors proposed Model 2 to analyze Motor B in ODP configuration. Complete details and results about Motor B analyzed with Model 2 can be found in [7]. For clarity, in Fig.18 the forced convection heat transfer coefficient estimated using Model 2 is compared with the same coefficient calculated through Model 1. It is possible to observe that the estimated values $h_{\text{Forced convection}}$ when the openings are open (curve “(a)-Model 2”) are comparable with the values obtained for Motor B in TEFC configuration and with positioned end rings (line “(b)-Model 1”). This result confirms the validity of the proposed experimental approach.

VII. CONCLUSIONS

The paper reports measurement campaign results concerning different cooling arrangements for induction motor endwindings. In particular, the impact of the frame openings and of the rotor end ring fins on the endwinding cooling is analyzed and quantified by means of two prototypes with nylon rotors. The measured overtemperatures have been used to estimate the heat transfer coefficients concerning the thermal transfer between endwindings and external frame, with respect to the considered cooling arrangements. The reported results confirm the reliability of the proposed approach and allow the calculation of the end space region thermal resistances to be used in electrical motor thermal networks.

ACKNOWLEDGMENTS

The authors would like to thank Alan Barker, Steve Ruffing and Alan Crapo of Emerson Motors, St. Louis, USA, for the support of this project. The authors would also like to acknowledge the support from Prof. TJE Miller Director of the *SPEED* Consortium, Glasgow, UK.

REFERENCES

- [1] A. Boglietti, A. Cavagnino, D. Staton, M. Shanel, M. Mueller, C. Mejuto “Evolution and Modern Approaches for Thermal Analysis of Electrical Machines”, *Trans. on Industrial Electronics*, Vol. 56, No. 3, March 2009, pp.871-882.
- [2] A. Boglietti, A. Cavagnino, “Analysis of the Endwinding Cooling Effects in TEFC Induction Motors”, *Transactions on Industry Applications*, Vol. 43, No. 5, Sept.-Oct. 2007, pp.1214 – 1222.
- [3] A. Boglietti, A. Cavagnino, M. Parvis, A. Vallan, “Evaluation of radiation thermal resistances in industrial motors”, *Trans. on Industry Applications*, Vol. 42, No. 3, May/June 2006, pp. 688-693.
- [4] J. Muggleston, S.J. Pickering, D. Lampard, “Effect of Geometry Changes on the Flow and Heat Transfer in the End Region of a TEFC Induction Motor”, 9th IEE Intl. Conf. Electrical Machines & Drives, Canterbury, UK, Sept 1999.
- [5] M.A Valenzuela, J.A. Tapia, “Heat Transfer and Thermal Design of Finned Frames for TEFC Variable Speed Motors”, Conf. Rec. IECON07, 6-10 November 2006, Paris, France.
- [6] C. Micallef, S.J. Pickering, K.A. Simmons, K.J. Bradley, “An Alternative Cooling Arrangement for the End Region of a Totally Enclosed Fan Cooled (TEFC) Induction Motor”, IEE Conf. Rec. PEMD 08, 3-5 April 2008, York, UK.
- [7] A. Boglietti, A. Cavagnino, D. Staton, M. Popescu, C. Cossar, M.I. McGilp, “End Space Heat Transfer Coefficient Determination for Different Induction Motor Enclosure Types”, *Trans. on Industry Applications*, Vol. 45, No. 3, May/June 2009, pp. 929-937.